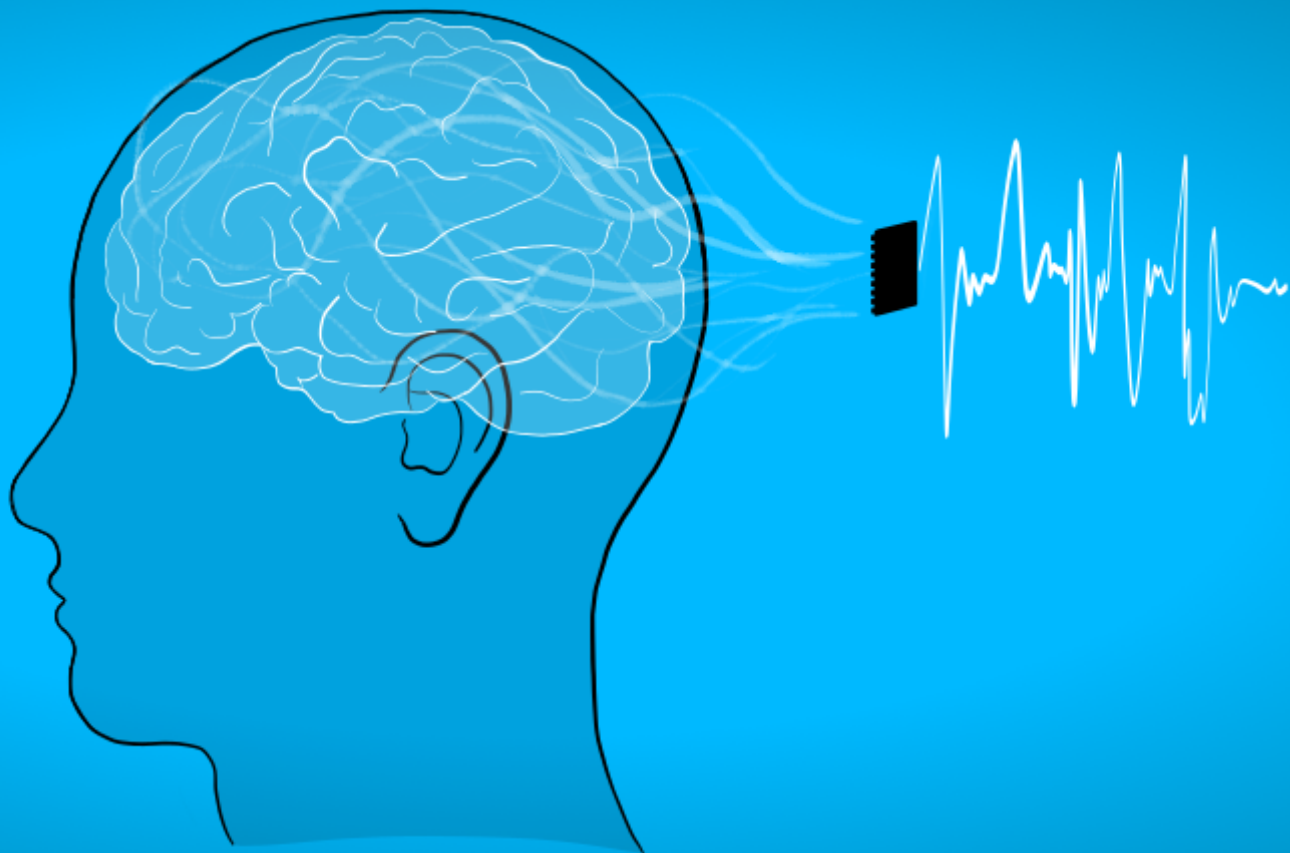


# Design of Flexible Dry CNT/PDMS Electrodes for In-ear EEG

The Effect of Microstructures on Electrode  
Performance

P. Burgar

Master of Science Thesis





# Design of Flexible Dry CNT/PDMS Electrodes for In-ear EEG

The Effect of Microstructures on Electrode Performance

by

Patricija Burgar

to obtain the degree of Master of Science in Biomedical Engineering  
at the Delft University of Technology.

Student number: 5268648  
Project duration: December 1, 2021 – September 2, 2022  
Thesis committee: Dr. D. G. Muratore, TU Delft, supervisor  
Dr. A. Rwei, TU Delft, supervisor  
Prof. dr. ir. W. A. Serdijn, TU Delft  
Dr. L. Peternel, TU Delft

An electronic version of this thesis is available at <http://repository.tudelft.nl/>.



## ACKNOWLEDGEMENTS

*During this thesis I had the opportunity to explore an interesting topic and meet many inspiring people from very different fields of research. I learned a lot from all of them and I appreciated their valuable input that shaped this thesis into its final form.*

*First, I would like to thank my supervisors, Dr. Dante Muratore and Dr. Alina Rwei for guiding me in the crucial moments and being available for discussions at all times throughout the project. They gave me the freedom to steer this thesis in the direction I wanted and made it a memorable experience. Next, I would like to thank Ida Kokalari and Erik Chen for helping me find my way around the lab and for sharing their knowledge on material fabrication and characterization. Furthermore, I must thank Brian Nanhekhan for going over and beyond in finding the right equipment for my testing setup.*

*Most importantly, I want to thank my partner, Corrado for motivating me at all times, and pushing me beyond my limits when I needed it. Special thanks go to my family, for always believing in me and supporting me in reaching my goals. Finally, I must thank my flatmates and friends for making these past months an unforgettable experience.*

*Patricija Burgar  
Delft, August 2022*

**Abstract**—In-ear EEG is a discreet and convenient method for monitoring EEG by placing the electrodes in the ear canal. This enables everyday monitoring outside of clinical environments in contrast to generally used scalp EEG with wet electrodes. This thesis proposes and describes the design of novel flexible dry CNT/PDMS electrodes with short pins, long pins, and a snake pattern. These dry electrodes make use of microstructures to improve electrode-skin impedance (ESI) by enlarging the effective contact area. In the composite fabrication process, SEM is used to optimize CNT dispersion which plays a significant role in the impedance of the material. The performance of the proposed dry electrodes is evaluated in comparison to conventionally used wet Ag/AgCl electrodes. Electrode impedance measurements show the superior performance of CNT/PDMS electrodes with microstructures with lower aspect ratios. This is confirmed by ESI measurements, which show a 49 % improvement at 10 Hz for the electrode with short pins compared to the electrode with long pins, and a further 53 % improvement for electrodes with the snake pattern. This makes the latter comparable to wet electrodes. Moreover, normalization by the projected surface area shows significantly lower ESI at low frequencies for dry CNT/PDMS electrodes with a snake pattern compared to wet electrodes. ESI of the dry electrode at 10 Hz is  $30 \text{ k}\Omega \text{ cm}^2$ , one order of magnitude lower than for wet electrodes. At 1 kHz the ESI is  $9.9 \text{ k}\Omega \text{ cm}^2$ , which is comparable to wet electrodes. Finally, ASSR tests show comparable suitability of dry CNT/PDMS electrodes and wet electrodes for in-ear EEG monitoring, suggesting that the proposed dry CNT/PDMS electrodes are a viable solution for in-ear EEG applications.

**Index Terms**—Flexible CNT/PDMS electrodes, In-ear EEG, Biosignal acquisition, Dry electrodes, Uniform CNT dispersion

## I. INTRODUCTION

Electroencephalography (EEG) is a record of electrical activity in the brain, typically detected by the electrodes placed on the surface of the skin. It can be used in a variety of applications, most commonly for detecting epilepsy, drowsiness level or in brain-computer interfaces (BCI) [1] [2]. For most applications, long-term monitoring is required, which is currently limited by the bulky devices and cumbersome application procedure of the conventional scalp EEG systems. The standard practice for EEG monitoring is using wet silver/silver chloride (Ag/AgCl) electrode arrays placed on the scalp [3]. This is usually performed in a clinical environment, where electrodes are mounted by trained personnel. The application procedure is time-consuming, as it requires skin preparation and adding gel to each of the electrodes. Additionally, the gel dries out over time which influences the signal quality and leaves dried residues on the scalp. Therefore, a new approach has recently been proposed, where EEG is measured from the ear canal (in-ear EEG) using dry electrodes.

In-ear EEG has several advantages, such as reduced interference from external electrical fields due to the ear canal being an enclosed cavity [4]. Also, in-ear EEG monitoring is more discrete and convenient than conventional scalp EEG (see Fig. 1). It can be worn as an earphone, which makes it a promising solution for more comfortable

long-term monitoring. During the in-ear EEG monitoring, electrodes are normally placed in the ear canal and the concha [5] [6] [7]. Additionally, the surface potentials on the outer ear have been determined based on a computational model and showed that the ear canal is the optimal location for source electrodes and the concha for reference electrodes [8].

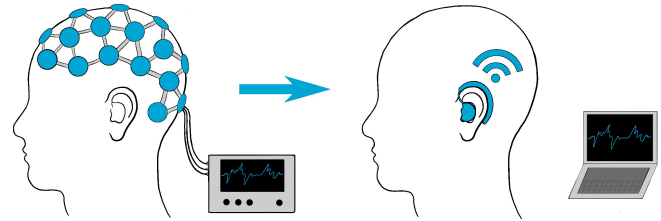


Fig. 1. Schematic model showing the transition from scalp EEG to in-ear EEG.

Recently dry electrodes are being researched due to their convenience and suitability for long-term monitoring. This type of electrode does not require the use of conductive gel. As shown in Fig. 2, the lack of gel reduces the effective electrode-skin contact area in the case of dry electrodes. This decrease leads to one or two orders of magnitude higher electrode-skin impedance (ESI) compared to wet electrodes, which normally exhibit ESI in the range of  $5 \text{ k}\Omega$  at 50 Hz [7]. However, eliminating the use of gel leads to a more stable ESI over time and an easier application procedure. This makes them a preferred option for use in wearable, long-term monitoring devices. Dry electrodes rely on maintaining good skin contact through either an attachment system exerting pressure on the electrodes or the self-adhesive properties of the electrode itself.

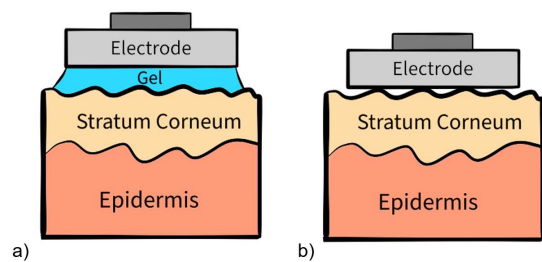


Fig. 2. Schematic model of electrode-skin interface for a) wet and b) dry electrodes [9]

Dry electrodes can be divided into (i) microneedles, (ii) textile-based electrodes, (iii) rigid metal-coated electrodes, and (iv) flexible polymer-based electrodes. Microneedles are invasive electrodes that can penetrate the Stratum Corneum, the outermost layer of skin [11][12][13][14]. This results in a low ESI, comparable to that of wet electrodes. Nevertheless, the microneedles are prone to breakage, especially when inserting them in the ear canal. Textile-based electrodes are commonly used as semi-dry electrodes as they usually rely

TABLE I  
Dry in-ear EEG systems overview

	[5]	[6]	[7]	[10]
<b>Electrode material</b>	Ag coated	Highly porous Pt	IrO <sub>2</sub> on Ti	AgNW/CNT/PDMS
<b>Used techniques</b>	Surface roughening, flexible cantilevers	Porous surface	Etched surface, flexible joint	Combining conductive fillers, flexible electrode
<b>Number of electrodes</b>	4 source + 2 ref.	4 source + 2 ref.	3 source + 3 ref.	4 source + 2 ref.
<b>Size of electrodes</b>	60 mm <sup>2</sup>	7 mm <sup>2</sup>	9.6 mm <sup>2</sup>	/
<b>Earpiece</b>	Flexible generic	Rigid custom	Flexible custom	Generic
<b>Impedance</b>	392 kΩ at 50 Hz	100* kΩ at 50 Hz	435 kΩ at 50 Hz	100* kΩ at 50 Hz

\* Approximate value

on absorbing sweat [15][16] or added saline solution [17] [18] to achieve ESI comparable to wet electrodes. However, the lack of sweat glands in the ear canal [19], makes textile-based electrodes less suitable for in-ear EEG applications. Rigid metal-coated electrodes are durable and convenient to use. The metal layer can be spray coated or deposited on top of a rigid structure [6] [7]. These electrodes are commonly used as in-ear EEG electrodes. However, the effective electrode-skin contact area is normally lower than the one of flexible electrodes, due to the limited deformability of the material [20]. Flexible electrodes are normally based on polymers in combination with conductive coating [21] or fillers [10] [22]. Their flexibility leads to better skin adherence which increases the effective electrode-skin contact area. This can be further improved by adding a porous top layer [20] or microstructures to the electrode surface. Some examples of microstructures include pillars [20] [23] [24], pyramid structures [25] or octopus-inspired structures [26]. These structures contribute to a larger effective surface area and, in the case of octopus-inspired electrodes, better adhesion to the skin. As specified by [23], microstructured flexible electrodes exhibited even lower ESI than flat flexible electrodes. This makes flexible electrodes with microstructures a promising solution for in-ear EEG applications.

Recently, several techniques for dry electrodes for in-ear EEG systems have been developed. It has been shown that placing flexible electrodes spray-coated with silver (Ag) on flexible cantilevers pressing against the skin ensures good electrode-skin contact [5]. The ESI can be further improved by enlarging the effective surface area of the electrode through surface treatment, such as surface roughening and plasma treatment [5]. Similarly, using highly porous platinum (Pt) electrodes, fabricated by electrodeposition, has been shown to enlarge the effective contact area and reduce ESI [6]. Furthermore, attaching the electrodes to a custom-made earpiece resulted in improved electrode-skin contact [6]. Next, coating the etched titanium (Ti) surface with iridium oxide (IrO<sub>2</sub>) leads to an enlarged surface area of the electrode and a low ESI [7]. The ESI can be

further improved by placing the electrodes on a custom earpiece with a flexible joint between the ear canal and the concha part, which ensures a good electrode-skin contact [7]. Finally, it has been shown that using a combination of carbon nanotubes (CNTs) and silver nanowires (AgNWs) as fillers in polydimethylsiloxane (PDMS) leads to a low impedance of the composite [10]. ESI can be improved by using a thin layer of this conductive composite attached to a flexible generic earpiece through a layer of gold [10]. Table I gives an overview of the current most relevant systems using dry electrodes.

This thesis presents the design of a flexible dry CNT/PDMS electrode for in-ear EEG that exploits microstructures to obtain an ESI similar to that of wet electrodes. Section II presents the main design considerations, the composite fabrication process, the mold design, and the assembly of the device. Section III introduces the characterization methods, which include SEM imaging, electrode impedance measurements, ESI measurements, and in-ear EEG tests. Section IV presents the experimental results and Section V discusses the main findings and future work.

## II. ELECTRODE DESIGN

Precise measurements are needed to detect changes in brain activity since the measured signal in EEG is in the range of 0.5 to 100  $\mu$ V [2]. When EEG is measured from the surface of the skin, the signal quality mainly depends on the ESI [7]. Therefore, multiple considerations have to be taken into account when designing an electrode for in-ear EEG. The most important factor influencing ESI and its long-term stability is the size of the effective contact area between the electrode and the skin. Increasing the effective contact area leads to a lower ESI [27]. This can be further improved by adding porous surfaces or microstructures to the electrode. According to [6], the surface area was increased by a factor of 40 after adding a porous layer. The second factor influencing ESI is the flexibility of the material. Flexible materials with elastic modulus similar to that of the skin enable better skin conformance and

stability compared to rigid materials, as they can deform together with the skin [20]. Good electrode-skin adherence is closely related to the size of the effective contact area and leads to lower ESI [28]. Finally, stable contact between the electrode and skin can be achieved by using an external system exerting pressure on the electrodes or through the self-adhesive properties of the electrode material. According to [27], the applied pressure leads to an ESI decrease by 82%. However, comfort should be considered when applying pressure, especially in long-term monitoring.

A research gap can be seen in the field of microstructured flexible electrodes for in-ear EEG. Such electrodes could potentially further improve ESI through added microstructures and flexibility of the material. That is especially due to ear canal curvatures which make it difficult to ensure good electrode-skin contact. Here, I propose an in-ear EEG system using flexible microstructured electrodes as in Fig.3, where the groups of conductive bendable pins in blue are representing the measuring electrodes. Simultaneously, the pins are used to anchor the earpiece in the ear canal while the concha part of the earpiece implements a reference electrode that presses against the ear. The flexible joint between the canal and concha part of the earpiece has already been presented by [7], however, the pressure exerted on the concha could be further improved by the proposed anchoring system.

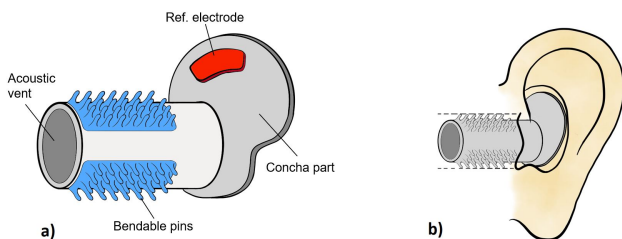


Fig. 3. Proposed concept solution for an in-ear EEG system.

### A. Composite fabrication

Flexible electrodes are normally fabricated either by using conductive polymers or non-conductive polymers in combination with conductive fillers. Most commonly, the conductive fillers are either metal (e.g., silver nanoparticles, silver nanowires, etc.) or carbon particles (e.g., graphene, carbon black, carbon nanotubes, etc.). In this work carbon nanotubes (CNTs) were used, due to their superior electrical properties [29] and biocompatibility when dispersed within a polymer [30]. Additionally, the CNTs are tangled randomly, which ensures good conductivity even when the polymer is bent or stretched [31]. Polydimethylsiloxane (PDMS) is used as the non-conductive polymer substrate, due to its wide usage in biomedical applications, biocompatibility, and flexibility. PDMS is a two-component polymer, which enables long CNT dispersion times before the composite

needs to be cured.

Due to van der Waals forces between CNTs, the main challenge in the electrode fabrication is achieving uniform dispersion of CNT within the PDMS [32]. This can be done by different techniques, such as shear mixing, mechanical stirring, or sonication. To increase the dispersion rate, a common solvent is often used in combination with those techniques [33][34]. Nevertheless, while a uniform dispersion of CNT increases the electrical conductivity of the composite, prolonged mechanical stress can lead to CNT shortening due to breakage. This leads to a decrease in the conductivity of the composite [32]. Here, a combination of sonication and a common solvent was used for electrode fabrication to obtain a good dispersion to CNTs breakage rate in a timely manner [35]. Isopropyl alcohol (IPA) is the common solvent of use, as it is an efficient and commonly used solvent for CNT dispersion. Additionally, it is convenient for handling compared to other, more toxic solvents, such as chloroform or toluene. Another factor affecting the electrical properties of CNT-based electrodes is the mass fraction of CNT in the polymer. The electrode impedance is decreasing with an increased CNT mass fraction, however, it has been shown that the impedance starts plateauing after 4 wt% mass fraction [33]. For that reason, a CNT mass fraction of 4.5 wt% was chosen for this application.

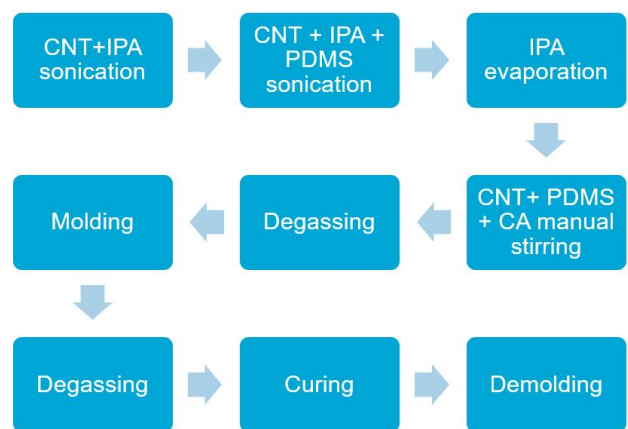


Fig. 4. Composite fabrication steps for the flexible dry electrodes.

The composite fabrication procedure consisted of many steps as shown in Fig. 4. First, multi-walled CNTs (Ossila BV, internal diameter: 5 - 2 nm, outer diameter: 40 nm, length: 10 - 30  $\mu\text{m}$ , purity: >95 %) were weighted in the fume hood, and mixed with IPA in 1:100 weight ratio. Using a bath sonicator, the solution was sonicated for 75 minutes. Second, the PDMS part-A was heated up to 40°C to decrease its viscosity, added to the CNT/IPA solution, and sonicated for another 5 minutes. After this step, CNTs were well dispersed in the solution and no big agglomerations were observed. Thirdly, the solution was placed in a vacuum

oven at 50°C until the IPA evaporated. This was confirmed by weighing the remaining solution in the vial. Next, the PDMS part-B was added to the composite in a 1:10 weight ratio and stirred manually for 5 minutes. The composite was placed in the vacuum pump to eliminate all the air bubbles (degassing). After fully degassing, the composite was poured into a mold, which was prepared by spray-coating with a mold release solution. The molded composite was again put in the vacuum pump overnight to eliminate the entrapped air bubbles. Finally, the molded composite was covered with a glass slide, which ensured a flat top surface, and cured in the oven at 70°C for 6 hours. The curing process was followed by demolding and cutting the sample into separate electrodes using a scalpel.

### B. Mold design

Each electrode is 4mm x 5mm (l x w) to safely fit four measuring electrodes in the ear canal without the risk of neighboring electrodes creating a short circuit. CAD models of the molds were created using AutoCAD Inventor software. The design of each type of mold was adapted to the type of process used for mold fabrication. Detailed designs and technical drawings can be found in the Appendix.

1) *Mold for electrode with pins:* Electrodes with pins were chosen based on the anchoring system described above (see Fig. 3). Each electrode has an array of pins covering the top part of the electrode. The diameter of each pin is 0.5 mm and the height is 1.5 mm, as the aspect ratio of 1:3 was found to be the optimal tradeoff between durability and flexibility ratio[36]. Each pin also has a rounded edge at the tip (shown in Appendix) to further increase durability and minimize possible damage during demolding [37]. The mold was fabricated using a micro-milling process to achieve the small vertical features - see Fig. 5. Micro-milling enables a smoother surface, minimizing friction during demolding and reducing pin damage. Whereas, in 3D printing, layers of the filament make the vertical surface rougher, which could result in more damaged pins.

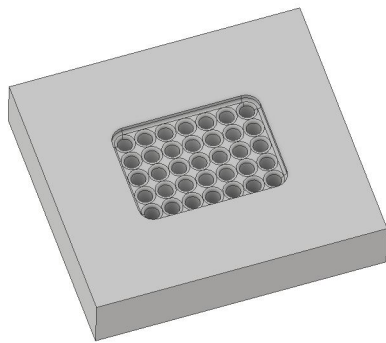


Fig. 5. 3D model of the first mold design.

2) *Mold for electrode with bio-inspired snakeskin pattern:* The second mold design was bio-inspired by a snakeskin pattern - see Fig. 6. The design of the pattern on the top side of the electrode resembles the scale shape of a snake, which enables movement in one direction and restricts movement in the other three directions by increased friction [38]. In this way, the design aims to achieve the same goal as the electrode with pins in terms of stability. However, it additionally avoids any potential problems with a high capacitive coupling between the long pins in the first mold design. As shown in Fig.6, each mold is suitable for fabricating four electrodes at once. The outer dimensions of each electrode remained the same as for the electrode with pins. For this mold, low-cost 3D printing was chosen as the optimal fabrication process as the indentations are shallower and wider. This results in easy demolding even in the case of rougher vertical parts of the mold.

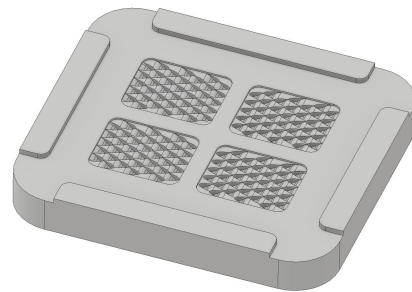


Fig. 6. 3D model of the second mold design.

### C. Device assembly

As mentioned in the introduction, the optimal position for measuring electrodes is in the ear canal. The size of the electrodes is suitable for placing up to four electrodes in each ear canal. After fabrication, both electrode types were assembled into an in-ear EEG measuring system using a commercially available soft earplug - see Fig. 7. Electrodes were attached to a wire using a conductive epoxy and taped to the earplug with double-sided tape while the wires were passed through the earplug. Additionally, a similar setup with wet electrodes was made as a comparison. Standard sintered Ag/AgCl electrodes for EEG with a 4 mm diameter were obtained from MedCaT BV and used in combination with a conductive gel Signa Gel. Setups with dry and wet electrodes were both used for in-ear measurements.

Also, a custom in-ear EEG device was assembled as a concept device, to show the feasibility of using four CNT/PDMS electrodes in one device. The custom earpiece was 3D printed by Formlabs. It consists of a custom 3D printed earpiece with a compartment for the electronics board and four electrodes - see Fig. 8. This device includes an acoustic vent and a pathway for wires to connect the electrodes with the electronics.

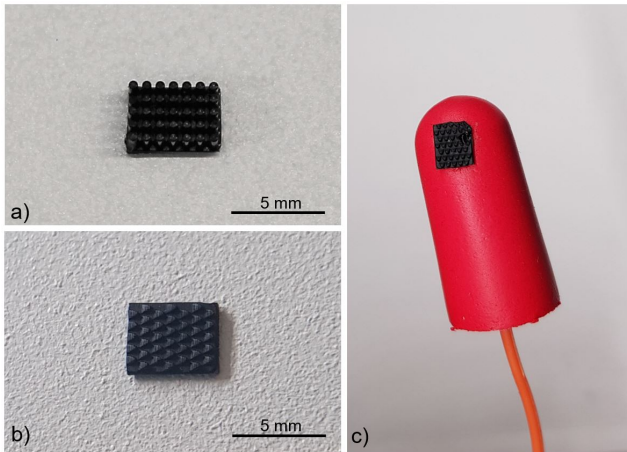


Fig. 7. Dry CNT/PDMS electrode with a) long pins and b) the snake pattern assembled into c) a generic in-ear EEG measuring system used for in-ear measurements.

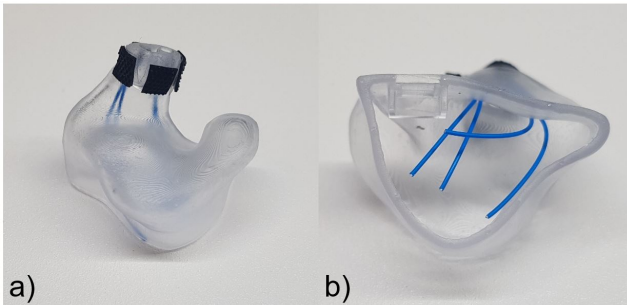


Fig. 8. Custom in-ear EEG device: a) side view of the device and b) bottom view of the PCB compartment.

### III. CHARACTERIZATION

#### A. SEM imaging

The dispersion of CNTs within PDMS is characterized using scanning electron microscopy (SEM). Uniformity of the dispersion plays a significant role in the electrical conductivity of the material. Thus, material fabrication steps can be optimized based on a cross-sectional SEM of the material. In that manner, uniformity of the dispersion throughout the material can be analyzed and possible shortening of the CNT can be seen. SEM was done on cross sections of four different samples, using JEOL JSM-6010LA Analytical Scanning Electron Microscope. First, a sample of PDMS and a sample of CNT/PDMS composite were coated with gold sputtering and placed in the sample holder. Next, the non-coated samples of PDMS and CNT/PDMS composite were added to the sample holder as shown in Fig.9. Additionally, SEM images of the non-coated electrode with pins were taken at a variety of magnifications to confirm the presence of CNTs in the tips of the pins and through the entire cross-section of the material.

#### B. Electrode impedance

Electrode impedance measurements are first used for the characterization of electrical properties of CNT/PDMS

electrodes. The impedance measurements were done in the range of 1 Hz to 100 Hz, which is in the range of brain activity [39]. For impedance measurements, the Zurich Instruments MFIA impedance analyzer was used in a two-terminal setup. This setup is preferred for electrodes with high impedance due to its simplicity and negligible measurement error at high impedance. The testing setup consisted of an electrode clamped between two Ag/AgCl plates. First, the impedance of two Ag/AgCl plates clamped together was measured and found to be negligible when compared to electrode impedance. Then, a set of measurements was taken for dry CNT/PDMS electrodes with long and short pins. The impedance of each electrode was measured five times to minimize the effect of measurement error due to electrode displacement and setup noise.

The process was repeated for dry CNT/PDMS electrodes with the snake pattern. In order to test the effect of sonication time on the impedance of the material, another set of dry CNT/PDMS electrodes with the snake pattern was produced with the total sonication time reduced to 20 minutes. The impedance was then measured for five electrodes with each sonication time used in the fabrication process. The impedance of each electrode was measured four times to minimize the effect of the measurement error.

#### C. Electrode-skin impedance

ESI was measured using Zurich Instruments MFIA impedance analyzer in the frequency range of 10 Hz to 1 kHz. This enabled comparison with other studies and provided information about the suitability of the proposed electrodes for EEG applications. Again, a two-terminal measuring setup was used due to the expected high impedance. For safety reasons, the electrode-skin impedance was measured on the forearm instead of in the ear canal, and the current range was limited to a maximum of 10 mA. Before testing, the skin of the forearm was cleaned with soap and dried. Impedance was first measured with two wet Ag/AgCl Skintact electrodes 4 cm apart, with a gel surface



Fig. 9. Prepared samples for SEM.

area of  $2 \text{ cm}^2$ . Impedance measurements were repeated five times. Later, one wet electrode was replaced by a dry CNT/PDMS electrode, and impedance measurements were repeated another five times. ESI was later calculated for each individual electrode. ESI measurements for wet electrode, dry CNT/PDMS electrode with long pins, dry CNT/PDMS electrode with short pins, and dry CNT/PDMS electrodes with the snake pattern were compared.

#### D. In-ear EEG

To characterize the suitability of dry CNT/PDMS electrodes for in-ear EEG application, the auditory steady-state response (ASSR) was measured. ASSR is a measurement of brain activity when listening to an auditory stimulus at a certain frequency. The response can be detected as a spurious tone in the EEG signal at the stimulation frequency. For this test, a frequency of 40 Hz is chosen, as it normally results in the most significant response [40]. For the ASSR measurements, the Cyton Biosensing board from OpenBCI was used in combination with dry CNT/PDMS electrodes with a snake pattern or wet Ag/AgCl electrodes inserted in the ear canal. The subject was sitting still while listening to an amplitude modulated 40 Hz auditory stimulus for 5 min. During this time the brain response was measured by two dry CNT/PDMS electrodes inserted in the right ear canal and a reference electrode placed on the mastoid of the opposite ear. A dry Ag/AgCl Earclip Electrode from OpenBCI was used as a reference electrode. Prior to inserting the measuring electrodes, the ear canal was cleaned using a cotton swab. Measurements with each electrode type were repeated five times. Finally, the measurements were analyzed and presented using a Python script.

## IV. RESULTS

### A. SEM imaging

Fig. 10 shows SEM images of four different samples. When comparing the gold-coated samples in Fig. 10(a) and Fig. 10(b), no significant difference can be seen between PDMS and CNT/PDMS samples, except for the dust particles on the surface of the samples. Whereas, a substantial difference is noticeable between the cross-sectional SEM images of non-coated samples. Fig 10(c) shows a non-coated PDMS sample, with no structures observable, except some grooves in the structures due to the cutting of the sample. Whereas, in Fig. 10(d), long CNT are clearly noticeable in white. This can be confirmed, due to the absence of such structures in the PDMS sample. CNTs appear to be well dispersed within the PDMS, with a few clusters of CNT present in some parts of the sample. Next, the dispersion within the sample can be observed in Fig. 11. From both, cross-sectional SEM and surface SEM images, the content of CNT appears to be well dispersed throughout the whole sample.

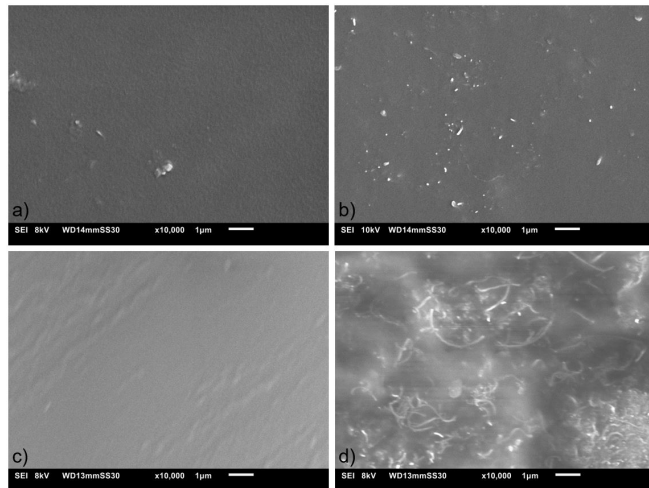


Fig. 10. SEM images of a) gold-coated PDMS, b) gold-coated CNT/PDMS, c) non-coated PDMS and d) non-coated CNT/PDMS sample.

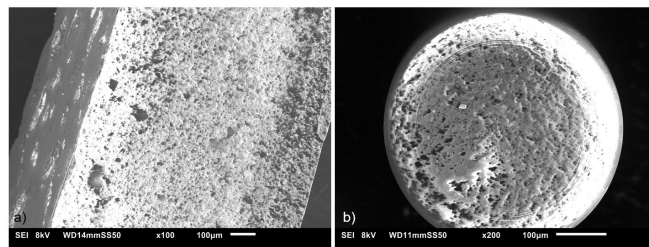


Fig. 11. SEM images of a) cross section and b) surface of a pin of the non-coated CNT/PDMS sample.

### B. Electrode impedance measurements

Firstly, the absolute impedance of the dry CNT/PDMS electrode with long pins and the electrode with short pins were compared - see Fig. 12. Both electrodes present similar impedance at low frequencies ( $\sim 5 \text{ M}\Omega$  at 1 Hz). However, the impedance at high frequencies increases more for the electrode with longer pins ( $\sim 8 \text{ M}\Omega$  at 100 Hz) than the electrode with short pins ( $\sim 5.5 \text{ M}\Omega$  at 100 Hz). Additionally, a high standard deviation can be observed for both electrodes, due to measurement noise and the effect of electrode displacement between different measurements.

Secondly, the absolute impedance of dry CNT/PDMS electrodes with the snake pattern was compared based on the sonication time used during fabrication. For electrodes A the total sonication time was 20 minutes and for electrodes B the total sonication time was 80 minutes. Fig. 13 shows that samples A (20 minutes sonication), exhibited overall a higher impedance than samples B (80 minutes sonication). The mean absolute impedance of samples A increased from around  $9 \text{ M}\Omega$  at 1 Hz to around  $15 \text{ M}\Omega$  at 100 Hz. Whereas, the mean absolute impedance of samples B increased from around  $4 \text{ M}\Omega$  at 1 Hz to around  $7 \text{ M}\Omega$  at 100 Hz. Moreover, a significantly higher standard deviation can be

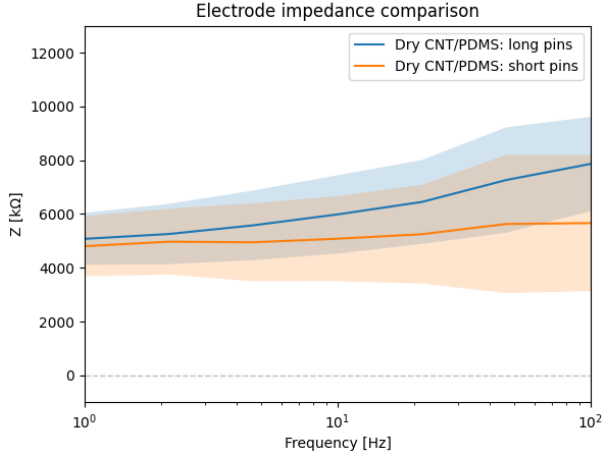


Fig. 12. Mean and standard deviation of absolute impedance values of electrode impedance measurements for dry CNT/PDMS electrode with long pins, and dry CNT/PDMS electrode with short pins.

observed for electrodes where a shorter sonication time was used, implying a less uniform dispersion among the samples.

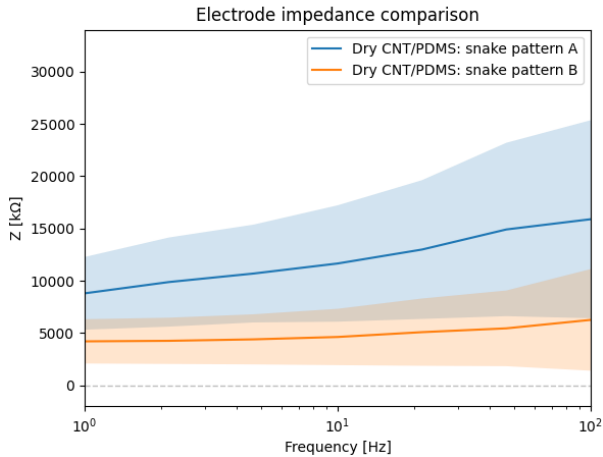
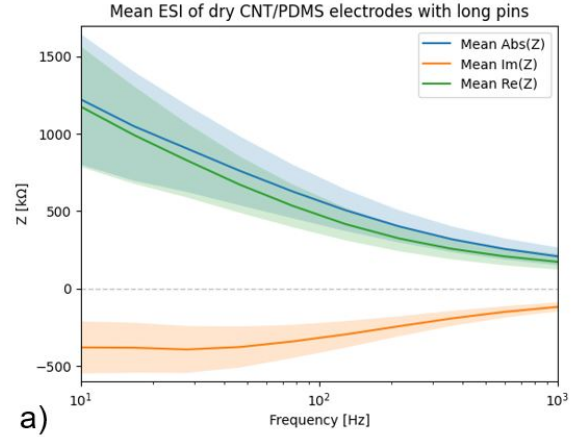


Fig. 13. Mean and standard deviation of absolute impedance values of electrode impedance measurements for dry CNT/PDMS electrode with snake pattern A (short sonication time), and dry CNT/PDMS electrode with snake pattern B (long sonication time).

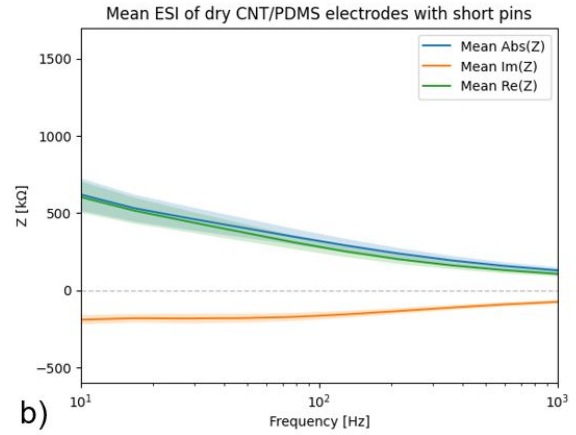
### C. Electrode-skin impedance measurements

In Fig. 14, the mean and standard deviation values of the absolute, imaginary, and real components of ESI for dry CNT/PDMS electrodes with long (Fig. 14(a)) and short pins (Fig. 14(b)) are compared (see Appendix for more details on ESI measurement setup). The mean absolute ESI is significantly higher for the electrode with long pins (1220 kΩ at 10 Hz) compared to the electrode with short pins (620 kΩ at 10 Hz). The difference in impedance is significantly smaller at higher frequencies. At 1 kHz

the mean absolute ESI of electrodes with long and short pins are 210 kΩ and 130 kΩ, respectively. Notably, the imaginary component of the ESI at lower frequencies is significantly higher for the electrode with long pins in comparison to the electrode with short pins. The difference at higher frequencies is smaller, which suggests that the dissimilarity is caused by a higher capacitive component present due to the larger parasitic coupling in the longer pins.



a)



b)

Fig. 14. Mean and standard deviation values of the absolute, real and imaginary component of ESI measurements for a) dry CNT/PDMS electrode with long pins and b) dry CNT/PDMS electrode with short pins.

Next, the mean absolute ESI values of dry CNT/PDMS electrodes with long pins, short pins, and a snake pattern are presented in Fig. 15 in comparison to the mean absolute ESI of a wet Ag/AgCl electrode. A further improvement in ESI can be seen in the case of the electrode with a snake pattern. The mean ESI for this electrode is only 290 kΩ at 10 Hz and 55 kΩ at 1 kHz. The ESI values are slightly higher than those of standard wet Ag/AgCl electrodes, which exhibited the mean ESI of 140 kΩ at 10 Hz and 4 kΩ at 1 kHz.

The surface areas of dry CNT/PDMS electrodes and the wet Ag/AgCl electrode are different, which has an effect on the measured ESI. Hence, the mean ESI values were normalized by the projected area of the electrodes. The contact area used for normalization is not considering

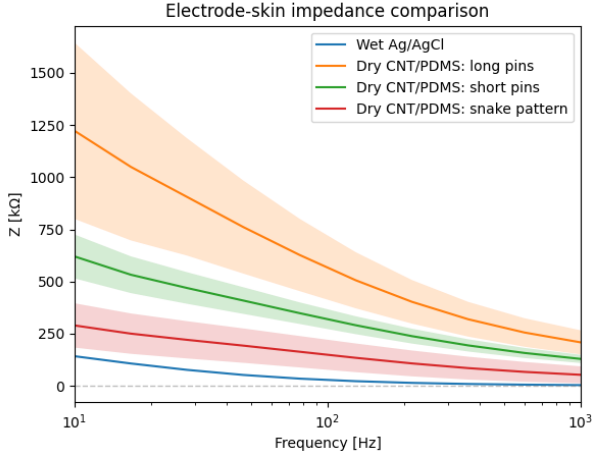


Fig. 15. Mean and standard deviation values of the electrode-skin impedance measurements for wet Ag/AgCl, dry CNT/PDMS electrode with long pins, dry CNT/PDMS electrode with short pins, and dry CNT/PDMS electrode with snake pattern.

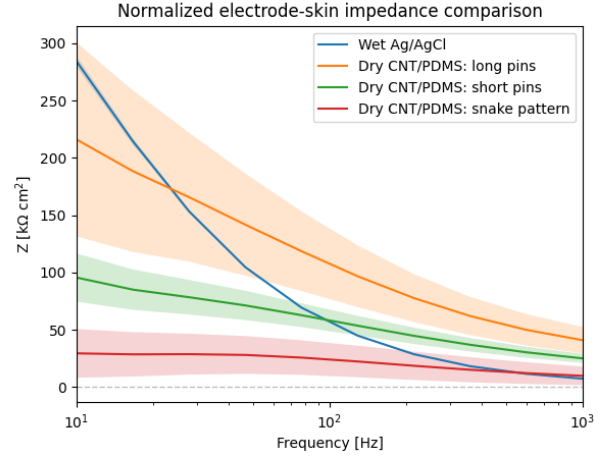


Fig. 16. Projected area normalized mean and standard deviation values of the electrode-skin impedance measurements for wet Ag/AgCl, dry CNT/PDMS electrode with long pins, dry CNT/PDMS electrode with short pins, and dry CNT/PDMS electrode with snake pattern.

the microstructures on the surface of the electrode, but only the global dimensions of the electrode. In this case, the projected area is  $20 \text{ mm}^2$  for all dry CNT/PDMS electrodes and  $2 \text{ cm}^2$  for the wet Ag/AgCl electrode. This normalization was chosen because the size of in-ear EEG electrodes is mainly limited by the global dimensions of the electrodes. The normalized results are shown in Fig. 16. A notably high ESI for the wet Ag/AgCl electrode can be observed at low frequencies, exceeding the ESI values of all types of dry CNT/PDMS electrodes presented. At 10 Hz, the normalized mean ESI values were  $285 \text{ k}\Omega \text{ cm}^2$ ,  $215 \text{ k}\Omega \text{ cm}^2$ ,  $95 \text{ k}\Omega \text{ cm}^2$ , and  $30 \text{ k}\Omega \text{ cm}^2$  for the wet Ag/AgCl electrode, the dry CNT/PDMS electrode with long pins, short pins, and a snake pattern, respectively. The ESI at higher frequencies remained the most stable for electrodes with short pins and a snake pattern, whereas in the case of wet electrodes and the dry electrode with long pins the decrease in ESI was more pronounced. At 1 kHz, the values were  $7.4 \text{ k}\Omega \text{ cm}^2$ ,  $41 \text{ k}\Omega \text{ cm}^2$ ,  $25 \text{ k}\Omega \text{ cm}^2$ , and  $9.9 \text{ k}\Omega \text{ cm}^2$  for the wet Ag/AgCl electrode, the dry CNT/PDMS electrode with long pins, short pins, and a snake pattern, respectively. Another important distinction between ESI values is the standard deviation of values for each type of electrode. The ESI measurements appear to be more consistent for the wet electrode in comparison to dry electrodes, due to lower measurement noise and reduced sensitivity to placement of the electrodes when using gel.

#### D. In-ear EEG measurements

The data obtained during in-ear EEG measurements was processed using a Python script. The mains interference frequency was first removed using a notch filter at 50 Hz. The data was then bandpass filtered in the range of 35 Hz to 45 Hz. Next, the power spectral density (PSD) per Hz was

calculated using `matplotlib.pyplot.specgram` function. The best example of ASSR result obtained by dry CNT/PDMS electrode with a snake pattern is shown in Fig. 17(a). From this graph a clear peak in the power spectrum can be seen at 40 Hz, showing the ASSR. Whereas, for wet Ag/AgCl electrodes, the results were visually not as significant. In the example from the same measurement, shown in Fig. 17(b), no clear peak can be seen at 40 Hz. Furthermore, the SNR was calculated as the ratio of the power at 40 Hz to the mean power of noise in the range of 35-45 Hz, excluding 40 Hz [7]. Results for five experiments are reported in Tab. II, showing a slightly higher SNR (1.56 dB) using the dry CNT/PDMS electrodes compared to the wet Ag/AgCl electrode (1.34 dB).

TABLE II  
ASSR at 40 Hz SNR values [dB]

	Dry CNT/PDMS el.	Wet Ag/AgCl el.
Measurement 1	1.41	0.88
Measurement 2	1.22	0.59
Measurement 3	1.63	1.49
Measurement 4	1.42	1.46
Measurement 5	2.12	2.28
Mean $\pm$ std	$1.56 \pm 0.31$	$1.34 \pm 0.58$

## V. DISCUSSION

In the previous sections, the design process of novel dry CNT/PDMS electrodes with microstructures was described. When it comes to the material fabrication process, a major challenge was achieving uniform dispersion of CNTs within PDMS. The sonication time was determined through trial and error, and IPA was shown to be the optimal common solvent. Initially, chloroform was considered as a common

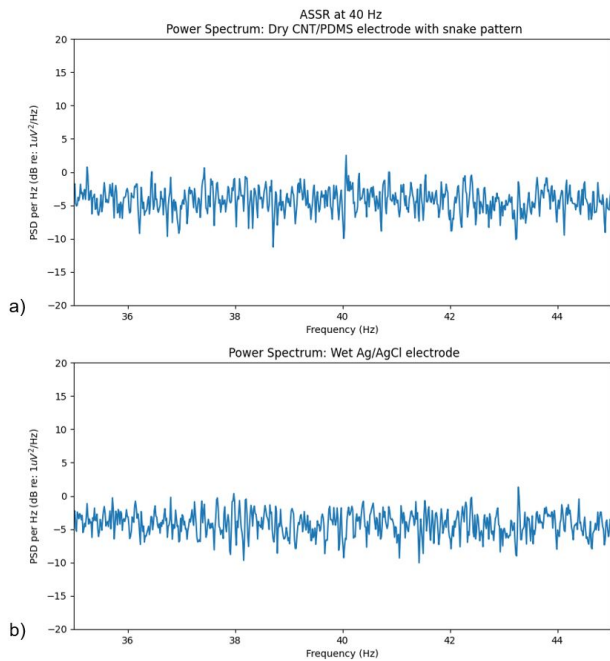


Fig. 17. Best example of ASSR measurement using 40 Hz amplitude modulated auditory stimulus with a) dry CNT/PDMS electrodes with snake pattern and b) wet Ag/AgCl electrodes.

solvent, due to better dispersion stability [41], however due to its toxicity and inadequate equipment for its evaporation, IPA has been chosen. Additionally, curing time was adjusted to 3 times longer than usual curing time for PDMS only [42] in order to obtain a fully cured composite. This is likely due to a high concentration of CNTs in the material, which decelerates the curing process. Additionally, the CNT mass fraction was limited to 4.5 wt% as the structural integrity of the material decreases at high mass fractions [33], which led to a higher rate of broken pins during the demolding process. This problem was less pronounced in the case of the snake pattern mold, due to lower friction during demolding. Thus, with this type of mold, composites with even higher CNT mass fractions could be used in the future. The electrical properties of the material could be further improved by adding a combination of different types of conductive fillers to the composite. According to [10], a combination of CNTs and AgNWs resulted in an electrode impedance decrease by two orders of magnitude, compared to a composite with only CNTs.

Next, the impedance of the material was measured by the clamping method, mainly to compare the effect of geometry and sonication times on the impedance of electrodes. In all measurements, a slight increase in impedance can be observed at high frequencies, which contradicts the expected electrode behavior. However, this can occur in impedance measurements, due to the inductance of the cables and parasitic capacitance [43]. When comparing the impedance of CNT/PDMS electrodes with long and short pins, the

difference is not very pronounced. At low frequencies, only a 5 % higher impedance can be observed in the case of the electrode with long pins. Whereas, the effect of sonication times on the impedance of the material was significantly more distinct. At low frequencies, electrodes with shorter sonication time exhibited a 52 % higher mean impedance than electrodes with longer sonication time. In addition, the standard deviation is significantly higher in the case of the shorter sonication time. This implies that 20 minutes of sonication was not adequate for a sufficient dispersion of CNT. For that reason, the conductive paths were not uniformly formed throughout the material [32] and the conductivity among the electrodes varied. Finally, it can be concluded that this type of measurement is more suitable for measuring the intrinsic properties of the material than its geometry. Especially, since ESI measurements confirmed a great influence of geometry on the electrical properties.

A clear difference between the mean ESI can be seen when comparing dry CNT/PDMS electrodes with long and short pins. The mean ESI of the electrode with long pins was two times higher than the mean ESI of the electrode with short pins in the whole frequency range. This could be due to a smaller effective surface area in the case of longer pins, as only the top part of pins is in contact with the skin, in contrast to the electrodes with short pins, where the vertical parts of the pins and the area between the pins add up to the effective contact area. Additionally, a lower imaginary component can be observed in the ESI of the electrode with longer pins. Since this is more pronounced in the low-frequency range, it most likely results from a capacitance formed between the long pins. Taking this effect into consideration, a new type of microstructures with a lower aspect ratio was designed.

Dry CNT/PDMS electrodes with the snake pattern exhibited even lower ESI than the previous two designs. The mean ESI at 10 Hz was 290 k $\Omega$ , which is in the range of ESI of other in-ear EEG electrodes, presented in Tab. I, and a 76% improvement in comparison to dry CNT/PDMS electrode with long pins. The mean ESI of wet Ag/AgCl electrode is in line with literature [31] at all measured frequencies, which confirms the suitability of the testing setup. Furthermore, snake pattern electrodes exhibited more consistent ESI results, as the standard deviation is clearly smaller than that of the long pin electrode. This shows that its ESI is less affected by the placement of the electrode and suggests better stability thanks to the snake pattern. The effect of the electrode placement on ESI is further reduced when using wet electrodes, as the gel ensures a stable electrode-skin contact and reduces sensitivity to measurement noise. Moreover, the comparison of the normalized ESI of the standard wet Ag/AgCl electrode and the newly developed dry electrodes showed a notable ESI change with frequency. This is most likely a result of using a conductive gel, which adds up to a higher capacitive component [9]. Based on this, we can see that the ESI of dry

CNT/PDMS electrodes is more stable over the frequency range from 10 Hz to 1 kHz. Therefore, the signal quality is more consistent in the frequency range compared to the signal measured by wet electrodes. Most importantly, the mean normalized ESI of the dry electrode with snake pattern at 10 Hz was only 30 k $\Omega$  cm<sup>2</sup>, which is an 89.5% improvement over the wet Ag/AgCl electrode. This makes the newly developed CNT/PDMS electrode with the snake pattern a suitable solution for EEG measurements.

The mean SNR of ASSR measurements is low for both dry CNT/PDMS and wet Ag/AgCl electrodes. In case of dry electrodes the mean SNR was 74 % and 89 % lower compared to other works using dry in-ear electrodes [5] [8]. Whereas, the mean SNR in the case of wet Ag/AgCl electrodes was 95 % lower than previously shown [44]. The reason for low SNR is probably the small size of electrodes, which leads to a high ESI. This also suggests that the Cyton board used for measuring ASSR, is most likely optimized for larger electrodes, which are normally used with the headset. Furthermore, a slight difference can be observed between the mean SNR of the measurements with dry (1.56 dB) and wet (1.34 dB) electrodes. This could be due to better adherence to the skin and lower ESI in the case of flexible dry electrodes. The ASSR measurements could be further improved by using a customized earpiece, which would ensure a better contact between the electrode and skin.

## VI. CONCLUSION

In this thesis, a novel flexible dry CNT/PDMS electrode was designed and evaluated for suitability for in-ear EEG applications. First, the concept idea was presented based on the main factors influencing the performance of dry contact electrodes and the current state-of-the-art. From a variety of materials used in flexible electrodes, CNT/PDMS composite was chosen as the optimal solution for this project. The most important fabrication steps of this composite were then identified and used for the fabrication of electrodes with three types of microstructures. Furthermore, the electrodes were characterized by SEM imaging, electrode impedance measurements by clamping the electrode between two metal plates, and ESI measurements. Through those methods, the effect of geometry and sonication time were compared. Microstructures with a lower aspect ratio showed favorable performance and resulted in ESI closer to that of the wet Ag/AgCl electrode. The best results were obtained from the dry CNT/PDMS electrode with the snake pattern, where after normalization, the ESI was lower than that of the wet Ag/AgCl electrode. Furthermore, the suitability of the final prototype of the electrode with a snakeskin pattern for EEG application was validated with an ASSR test.

In future work, a customized earpiece could be used for in-ear measurements. This would ensure a better ESI due to an improved electrode-skin contact, as the electrodes would be pressed against the skin more uniformly. Additionally, the electronics board could be integrated into the customized

earpiece to enable long-term measurements and convenience of use. Furthermore, the impedance of the electrodes could be improved by adding a combination of different conductive fillers into the non-conductive polymer. Finally, more in-ear EEG tests, such as ASSR should be performed on a variety of subjects to obtain more statistically relevant results.

## REFERENCES

- [1] A. J. Casson, D. C. Yates, S. J. Smith, J. S. Duncan, and E. Rodriguez-Villegas, "Wearable electroencephalography," *IEEE Engineering in Medicine and Biology Magazine*, vol. 29, no. 3, pp. 44–56, May 2010, Conference Name: IEEE Engineering in Medicine and Biology Magazine, ISSN: 1937-4186. DOI: 10.1109/MEMB.2010.936545.
- [2] M. Teplan, "FUNDAMENTALS OF EEG MEASUREMENT," *MEASUREMENT SCIENCE REVIEW*, vol. 2, p. 11, 2002.
- [3] V. Mihajlović, B. Grundlehner, R. Vullers, and J. Penders, "Wearable, wireless EEG solutions in daily life applications: What are we missing?" *IEEE Journal of Biomedical and Health Informatics*, vol. 19, no. 1, pp. 6–21, Jan. 2015, Conference Name: IEEE Journal of Biomedical and Health Informatics, ISSN: 2168-2208. DOI: 10.1109/JBHI.2014.2328317.
- [4] D. Looney, P. Kidmose, C. Park, *et al.*, "The in-the-ear recording concept: User-centered and wearable brain monitoring," *IEEE Pulse*, vol. 3, no. 6, pp. 32–42, Nov. 2012, Conference Name: IEEE Pulse, ISSN: 2154-2317. DOI: 10.1109/MPUL.2012.2216717.
- [5] R. Kaveh, J. Doong, A. Zhou, *et al.*, "Wireless user-generic ear EEG," *IEEE Transactions on Biomedical Circuits and Systems*, vol. 14, no. 4, pp. 727–737, Aug. 2020, Conference Name: IEEE Transactions on Biomedical Circuits and Systems, ISSN: 1940-9990. DOI: 10.1109/TBCAS.2020.3001265.
- [6] M. Eickenscheidt, P. Schäfer, Y. Baslan, C. Schwarz, and T. Stieglitz, "Highly porous platinum electrodes for dry ear-EEG measurements," *Sensors*, vol. 20, no. 11, p. 3176, Jan. 2020, Number: 11 Publisher: Multidisciplinary Digital Publishing Institute. DOI: 10.3390/s20113176. [Online]. Available: <https://www.mdpi.com/1424-8220/20/11/3176> (visited on 11/29/2021).
- [7] S. L. Kappel, M. L. Rank, H. O. Toft, M. Andersen, and P. Kidmose, "Dry-contact electrode ear-EEG," *IEEE Transactions on Biomedical Engineering*, vol. 66, no. 1, pp. 150–158, Jan. 2019, Conference Name: IEEE Transactions on Biomedical Engineering, ISSN: 1558-2531. DOI: 10.1109/TBME.2018.2835778.
- [8] S. L. Kappel, S. Makeig, and P. Kidmose, "Ear-EEG forward models: Improved head-models for ear-EEG," *Frontiers in Neuroscience*, vol. 13, 2019, ISSN: 1662-453X. [Online]. Available: <https://www.frontiersin.org/article/10.3389/fnins.2019.00943> (visited on 02/08/2022).

- [9] Y. Fu, J. Zhao, Y. Dong, and X. Wang, "Dry electrodes for human bioelectrical signal monitoring," *Sensors*, vol. 20, no. 13, p. 3651, Jan. 2020, Number: 13 Publisher: Multidisciplinary Digital Publishing Institute. DOI: 10.3390/s20133651. [Online]. Available: <https://www.mdpi.com/1424-8220/20/13/3651> (visited on 12/07/2021).
- [10] J. H. Lee, J.-Y. Hwang, J. Zhu, *et al.*, "Flexible conductive composite integrated with personal earphone for wireless, real-time monitoring of electrophysiological signs," *ACS Applied Materials & Interfaces*, vol. 10, no. 25, pp. 21 184–21 190, Jun. 27, 2018, Publisher: American Chemical Society, ISSN: 1944-8244. DOI: 10.1021/acsami.8b06484. [Online]. Available: <https://doi.org/10.1021/acsami.8b06484> (visited on 01/10/2022).
- [11] J. K. Radhakrishnan, S. Nithila, S. N. Kartik, T. Bhuvana, G. U. Kulkarni, and U. K. Singh, "A novel, needle-array dry-electrode with stainless steel micro-tips, for electroencephalography monitoring," *Journal of Medical Devices*, vol. 12, no. 4, Sep. 21, 2018, ISSN: 1932-6181. DOI: 10.1115/1.4041227. [Online]. Available: <https://doi.org/10.1115/1.4041227> (visited on 01/10/2022).
- [12] W. C. Ng, H. L. Seet, K. S. Lee, *et al.*, "Microspike EEG electrode and the vacuum-casting technology for mass production," *Journal of Materials Processing Technology*, vol. 209, no. 9, pp. 4434–4438, May 1, 2009, ISSN: 0924-0136. DOI: 10.1016/j.jmatprotec.2008.10.051. [Online]. Available: <https://www.sciencedirect.com/science/article/pii/S092401360800770X> (visited on 01/10/2022).
- [13] L. Ren, S. Xu, J. Gao, *et al.*, "Fabrication of flexible microneedle array electrodes for wearable bio-signal recording," *Sensors*, vol. 18, no. 4, p. 1191, Apr. 2018, Number: 4 Publisher: Multidisciplinary Digital Publishing Institute. DOI: 10.3390/s18041191. [Online]. Available: <https://www.mdpi.com/1424-8220/18/4/1191> (visited on 01/10/2022).
- [14] R. Wang, X. Jiang, W. Wang, and Z. Li, "A microneedle electrode array on flexible substrate for long-term EEG monitoring," *Sensors and Actuators B: Chemical*, vol. 244, pp. 750–758, Jun. 2017, ISSN: 09254005. DOI: 10.1016/j.snb.2017.01.052. [Online]. Available: <https://linkinghub.elsevier.com/retrieve/pii/S092540051730059X> (visited on 01/10/2022).
- [15] L. Shu, T. Xu, and X. Xu, "Multilayer sweat-absorbable textile electrode for EEG measurement in forehead site," *IEEE Sensors Journal*, vol. 19, no. 15, pp. 5995–6005, Aug. 2019, Conference Name: IEEE Sensors Journal, ISSN: 1558-1748. DOI: 10.1109/JSEN.2019.2912667.
- [16] C.-T. Lin, L.-D. Liao, Y.-H. Liu, I.-J. Wang, B.-S. Lin, and J.-Y. Chang, "Novel dry polymer foam electrodes for long-term EEG measurement," *IEEE Transactions on Biomedical Engineering*, vol. 58, no. 5, pp. 1200–1207, May 2011, Conference Name: IEEE Transactions on Biomedical Engineering, ISSN: 1558-2531. DOI: 10.1109/TBME.2010.2102353.
- [17] V. Goverdovsky, D. Looney, P. Kidmose, and D. P. Mandic, "In-ear EEG from viscoelastic generic earpieces: Robust and unobtrusive 24/7 monitoring," *IEEE Sensors Journal*, vol. 16, no. 1, pp. 271–277, Jan. 2016, Conference Name: IEEE Sensors Journal, ISSN: 1558-1748. DOI: 10.1109/JSEN.2015.2471183.
- [18] J. Löfhede, F. Seoane, and M. Thordstein, "Textile electrodes for EEG recording — a pilot study," *Sensors*, vol. 12, no. 12, pp. 16 907–16 919, Dec. 2012, Number: 12 Publisher: Multidisciplinary Digital Publishing Institute. DOI: 10.3390/s121216907. [Online]. Available: <https://www.mdpi.com/1424-8220/12/12/16907> (visited on 01/10/2022).
- [19] M. Stoeckelhuber, C. Matthias, M. Andratschke, *et al.*, "Human ceruminous gland: Ultrastructure and histochemical analysis of antimicrobial and cytoskeletal components," *The Anatomical Record Part A: Discoveries in Molecular, Cellular, and Evolutionary Biology*, vol. 288A, no. 8, pp. 877–884, 2006, \_eprint: <https://anatomypubs.onlinelibrary.wiley.com/doi/pdf/10.1002/ar.a.20356>. ISSN: 1552-4892. DOI: 10.1002/ar.a.20356. [Online]. Available: <http://onlinelibrary.wiley.com/doi/abs/10.1002/ar.a.20356> (visited on 02/07/2022).
- [20] F. Stauffer, M. Thielen, C. Sauter, *et al.*, "Skin conformal polymer electrodes for clinical ECG and EEG recordings," *Advanced Healthcare Materials*, vol. 7, no. 7, p. 1700994, 2018, \_eprint: <https://onlinelibrary.wiley.com/doi/pdf/10.1002/adhm.201700994>. ISSN: 2192-2659. DOI: 10.1002/adhm.201700994. [Online]. Available: <http://onlinelibrary.wiley.com/doi/abs/10.1002/adhm.201700994> (visited on 01/10/2022).
- [21] P. S. Das, H. S. Yoon, J. Kim, D. H. Kim, and J. Y. Park, "Simple fabrication method of an ultrasensitive gold micro-structured dry skin sensor for biopotential recording," *Microelectronic Engineering*, vol. 197, pp. 96–103, Oct. 5, 2018, ISSN: 0167-9317. DOI: 10.1016/j.mee.2018.06.005. [Online]. Available: <https://www.sciencedirect.com/science/article/pii/S016793171830217X> (visited on 01/10/2022).
- [22] A. A. Chlahawi, B. B. Narakathu, S. Emamian, B. J. Bazuin, and M. Z. Atashbar, "Development of printed and flexible dry ECG electrodes," *Sensing and Bio-Sensing Research*, vol. 20, pp. 9–15, Sep. 1, 2018, ISSN: 2214-1804. DOI: 10.1016/j.sbsr.2018.05.001. [Online]. Available: <https://www.sciencedirect.com/science/article/pii/S2214180418300254> (visited on 11/30/2021).
- [23] S. Kaitainen, A. Kutvonen, M. Suvanto, T. T. Pakkanen, R. Lappalainen, and S. Myllymaa, "Liquid silicone rubber (LSR)-based dry bioelectrodes: The effect of surface micropillar structuring and silver coating on contact impedance," *Sensors and Actuators A: Physical*, vol. 206, pp. 22–29, Feb. 1, 2014, ISSN: 0924-4247. DOI: 10.1016/j.sna.2013.11.020.

- [Online]. Available: <https://www.sciencedirect.com/science/article/pii/S0924424713005748> (visited on 01/10/2022).
- [24] P. Fiedler, L. T. Cunha, P. Pedrosa, *et al.*, “Novel TiN<sub>x</sub>-based biosignal electrodes for electroencephalography,” *Measurement Science and Technology*, vol. 22, no. 12, p. 124 007, Nov. 2011, Publisher: IOP Publishing, ISSN: 0957-0233. DOI: 10.1088/0957-0233/22/12/124007. [Online]. Available: <https://doi.org/10.1088/0957-0233/22/12/124007> (visited on 01/10/2022).
- [25] L. Shao, Y. Guo, W. Liu, T. Sun, and D. Wei, “A flexible dry electroencephalogram electrode based on graphene materials,” *Materials Research Express*, vol. 6, no. 8, p. 085 619, May 2019, Publisher: IOP Publishing, ISSN: 2053-1591. DOI: 10.1088/2053-1591/ab20a7. [Online]. Available: <https://doi.org/10.1088/2053-1591/ab20a7> (visited on 01/10/2022).
- [26] S. Chun, D. W. Kim, S. Baik, *et al.*, “Conductive and stretchable adhesive electronics with miniaturized octopus-like suckers against dry/wet skin for biosignal monitoring,” *Advanced Functional Materials*, vol. 28, no. 52, p. 1 805 224, 2018, eprint: <https://onlinelibrary.wiley.com/doi/pdf/10.1002/adfm.201805224>. ISSN: 1616-3028. DOI: 10.1002/adfm.201805224. [Online]. Available: <http://onlinelibrary.wiley.com/doi/abs/10.1002/adfm.201805224> (visited on 01/12/2022).
- [27] G. Li, S. Wang, and Y. Y. Duan, “Towards gel-free electrodes: A systematic study of electrode-skin impedance,” *Sensors and Actuators B: Chemical*, vol. 241, pp. 1244–1255, Mar. 31, 2017, ISSN: 0925-4005. DOI: 10.1016/j.snb.2016.10.005. [Online]. Available: <https://www.sciencedirect.com/science/article/pii/S0925400516316318> (visited on 11/30/2021).
- [28] C.-T. Lin, L.-D. Liao, Y.-H. Liu, I.-J. Wang, B.-S. Lin, and J.-Y. Chang, “Novel dry polymer foam electrodes for long-term EEG measurement,” *IEEE Transactions on Biomedical Engineering*, vol. 58, no. 5, pp. 1200–1207, 2011, ISSN: 0018-9294. DOI: 10.1109/TBME.2010.2102353.
- [29] G. Ruffini, S. Dunne, L. Fuentemilla, *et al.*, “First human trials of a dry electrophysiology sensor using a carbon nanotube array interface,” *Sensors and Actuators A: Physical*, vol. 144, no. 2, pp. 275–279, Jun. 15, 2008, ISSN: 0924-4247. DOI: 10.1016/j.sna.2008.03.007. [Online]. Available: <https://www.sciencedirect.com/science/article/pii/S0924424708001325> (visited on 01/10/2022).
- [30] H.-C. Jung, J.-H. Moon, D.-H. Baek, *et al.*, “CNT/PDMS composite flexible dry electrodes for long-term ECG monitoring,” *IEEE Transactions on Biomedical Engineering*, vol. 59, no. 5, pp. 1472–1479, May 2012, Conference Name: IEEE Transactions on Biomedical Engineering, ISSN: 1558-2531. DOI: 10.1109/TBME.2012.2190288.
- [31] J. Jung, S. Shin, and Y. T. Kim, “Dry electrode made from carbon nanotubes for continuous recording of bio-signals,” *Microelectronic Engineering*, vol. 203–204, pp. 25–30, Jan. 1, 2019, ISSN: 0167-9317. DOI: 10.1016/j.mee.2018.11.003. [Online]. Available: <https://www.sciencedirect.com/science/article/pii/S0167931718302272> (visited on 12/07/2021).
- [32] Y. Y. Huang and E. M. Terentjev, “Dispersion of carbon nanotubes: Mixing, sonication, stabilization, and composite properties,” *Polymers*, vol. 4, no. 1, pp. 275–295, Mar. 2012, Number: 1 Publisher: Molecular Diversity Preservation International, ISSN: 2073-4360. DOI: 10.3390/polym4010275. [Online]. Available: <https://www.mdpi.com/2073-4360/4/1/275> (visited on 03/23/2022).
- [33] J. H. Kim, J.-Y. Hwang, H. R. Hwang, *et al.*, “Simple and cost-effective method of highly conductive and elastic carbon nanotube/polydimethylsiloxane composite for wearable electronics,” *Scientific Reports*, vol. 8, no. 1, p. 1375, Jan. 22, 2018, Number: 1 Publisher: Nature Publishing Group, ISSN: 2045-2322. DOI: 10.1038/s41598-017-18209-w. [Online]. Available: <https://www.nature.com/articles/s41598-017-18209-w> (visited on 04/11/2022).
- [34] C. Fekiri, H. C. Kim, and I. H. Lee, “3d-printable carbon nanotubes-based composite for flexible piezoresistive sensors,” *Materials*, vol. 13, no. 23, p. 5482, Dec. 1, 2020, ISSN: 1996-1944. DOI: 10.3390/ma13235482. [Online]. Available: <https://www.mdpi.com/1996-1944/13/23/5482> (visited on 03/22/2022).
- [35] P.-C. Ma, N. A. Siddiqui, G. Marom, and J.-K. Kim, “Dispersion and functionalization of carbon nanotubes for polymer-based nanocomposites: A review,” *Composites Part A: Applied Science and Manufacturing*, vol. 41, no. 10, pp. 1345–1367, Oct. 1, 2010, ISSN: 1359-835X. DOI: 10.1016/j.compositesa.2010.07.003. [Online]. Available: <https://www.sciencedirect.com/science/article/pii/S1359835X10002009> (visited on 04/18/2022).
- [36] T. Kim, J. Park, J. Sohn, D. Cho, and S. Jeon, “Bioinspired, highly stretchable, and conductive dry adhesives based on 1d–2d hybrid carbon nanocomposites for all-in-one ECG electrodes,” *ACS Nano*, vol. 10, no. 4, pp. 4770–4778, Apr. 26, 2016, Publisher: American Chemical Society, ISSN: 1936-0851. DOI: 10.1021/acsnano.6b01355. [Online]. Available: <https://doi.org/10.1021/acsnano.6b01355> (visited on 02/24/2022).
- [37] D. C. Creton, “Prof. Dr.-Ing. S. Diebels,” p. 152,
- [38] D. L. Hu, J. Nirody, T. Scott, and M. J. Shelley, “The mechanics of slithering locomotion,” *Proceedings of the National Academy of Sciences*, vol. 106, no. 25, pp. 10 081–10 085, Jun. 23, 2009, Publisher: Proceedings of the National Academy of Sciences. DOI: 10.1073/pnas.0812533106. [Online]. Available: <http://www.pnas.org/doi/full/10.1073/pnas.0812533106> (visited on 08/06/2022).
- [39] P. A. Abhang, B. W. Gawali, and S. C. Mehrotra, “Technological basics of EEG recording and oper-

- ation of apparatus,” in *Introduction to EEG- and Speech-Based Emotion Recognition*, Elsevier, 2016, pp. 19–50, ISBN: 978-0-12-804490-2. DOI: 10.1016/B978-0-12-804490-2.00002-6. [Online]. Available: <https://linkinghub.elsevier.com/retrieve/pii/B9780128044902000026> (visited on 08/04/2022).
- [40] C. B. Christensen, S. L. Kappel, and P. Kidmose, “Auditory steady-state responses across chirp repetition rates for ear-EEG and scalp EEG,” in *2018 40th Annual International Conference of the IEEE Engineering in Medicine and Biology Society (EMBC)*, ISSN: 1558-4615, Jul. 2018, pp. 1376–1379. DOI: 10.1109/EMBC.2018.8512527.
- [41] T. Michel, M. Capasso, M. Cavusoglu, *et al.*, “Evaluation of porous polydimethylsiloxane/carbon nanotubes (PDMS/CNTs) nanocomposites as piezoresistive sensor materials,” *Microsystem Technologies*, vol. 26, Apr. 1, 2020. DOI: 10.1007/s00542-019-04636-4.
- [42] “Information about dow corning brand silicone encapsulants - PDF free download.” (), [Online]. Available: [https://businessdocbox.com/Green\\_Solutions/67460800-Information-about-dow-corning-brand-silicone-encapsulants.html](https://businessdocbox.com/Green_Solutions/67460800-Information-about-dow-corning-brand-silicone-encapsulants.html) (visited on 08/06/2022).
- [43] D. Dutra and P. Bertemes-Filho, “Extracting parasite effects of electrical bioimpedance measurements,” *Journal of Electrical Bioimpedance*, vol. 9, no. 1, pp. 115–122, Dec. 31, 2018, ISSN: 1891-5469. DOI: 10.2478/joeb-2018-0016. [Online]. Available: <https://www.ncbi.nlm.nih.gov/pmc/articles/PMC7852010/> (visited on 08/06/2022).
- [44] P. Kidmose, D. Looney, M. Ungstrup, M. L. Rank, and D. P. Mandic, “A study of evoked potentials from ear-EEG,” *IEEE Transactions on Biomedical Engineering*, vol. 60, no. 10, pp. 2824–2830, Oct. 2013, Conference Name: IEEE Transactions on Biomedical Engineering, ISSN: 1558-2531. DOI: 10.1109/TBME.2013.2264956.

APPENDIX

A. Technical drawings of molds

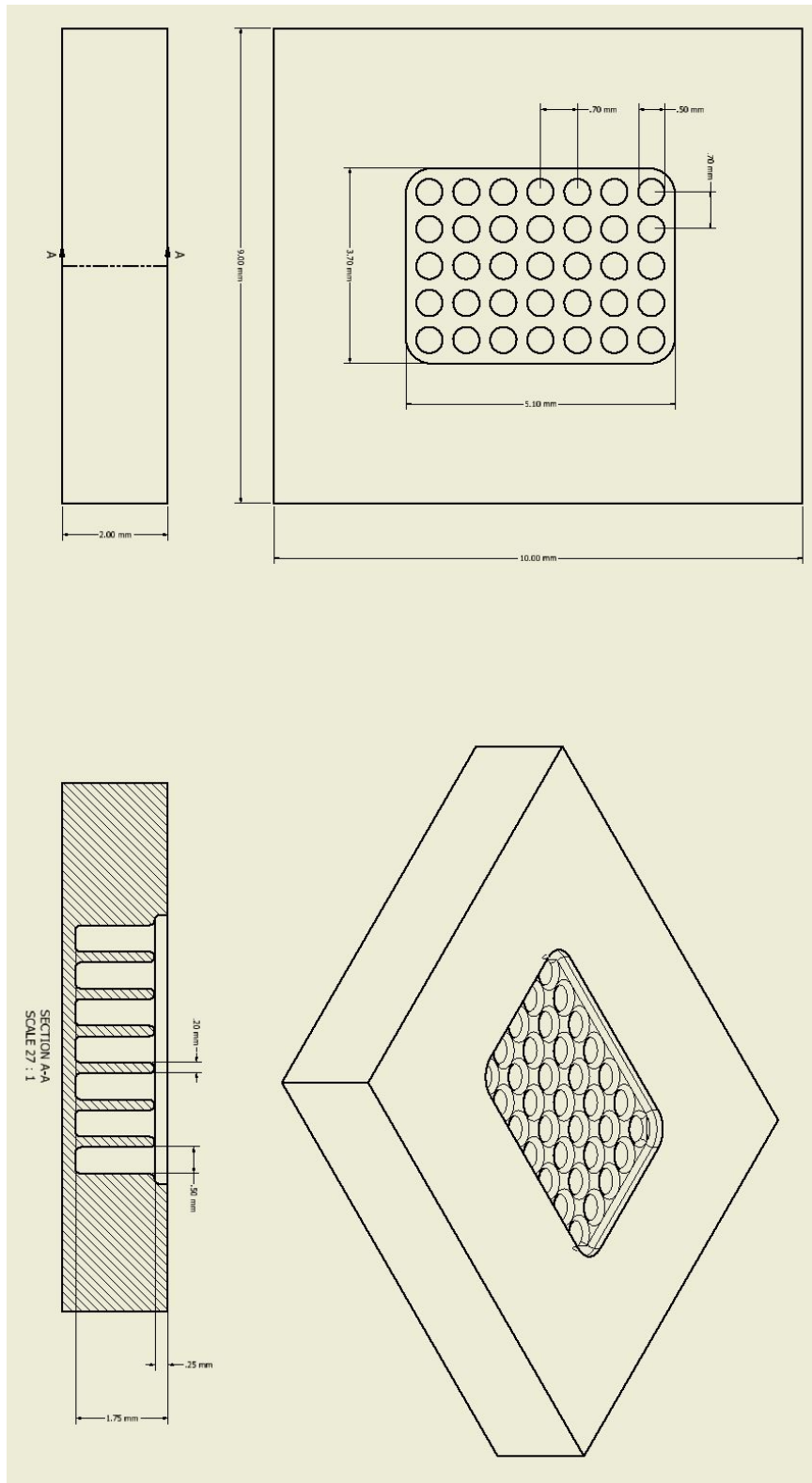


Fig. 18. Technical drawings of the mold for the electrode with pins.

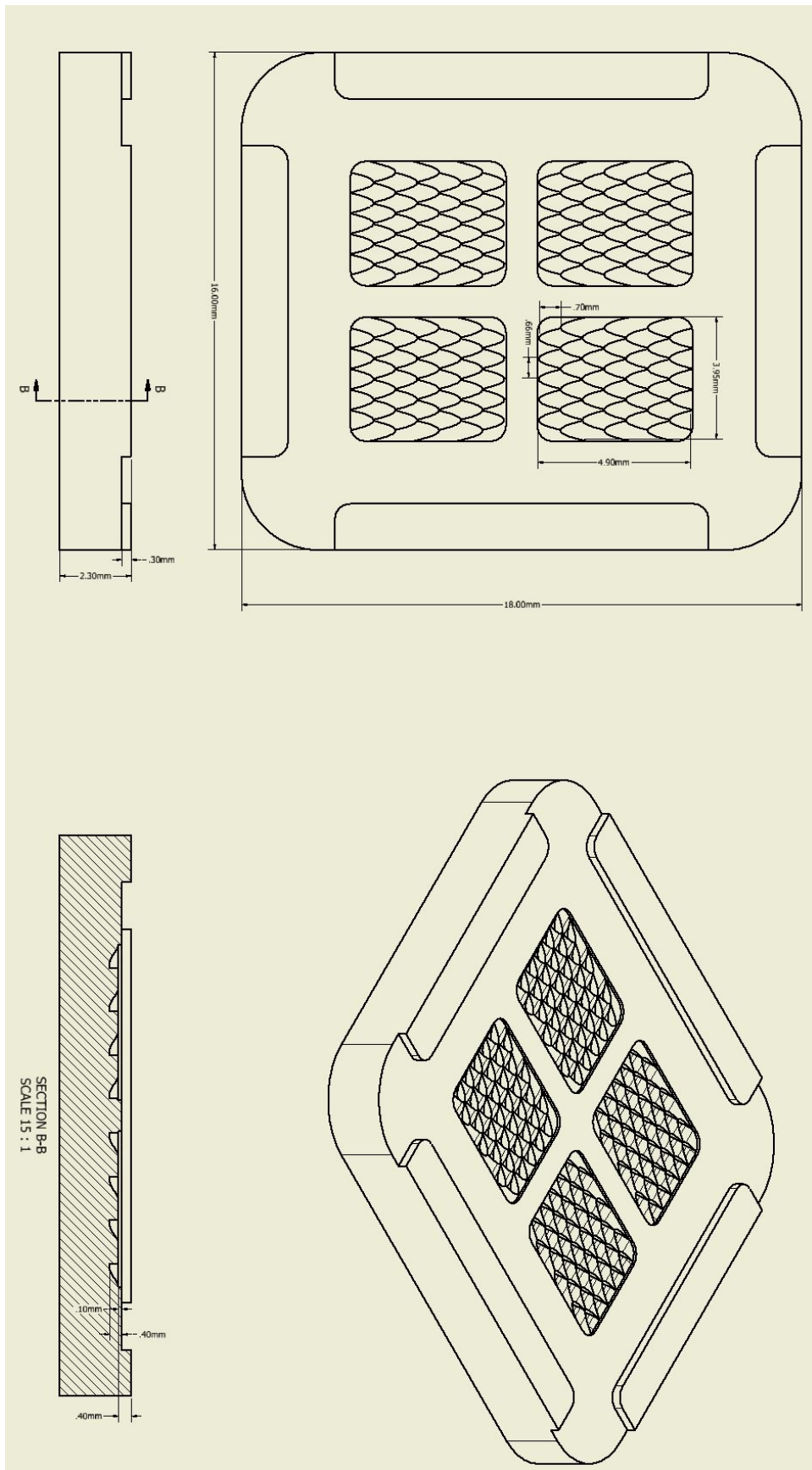


Fig. 19. Technical drawings of the mold for the electrode with the snake pattern.

B. CAD models of electrodes

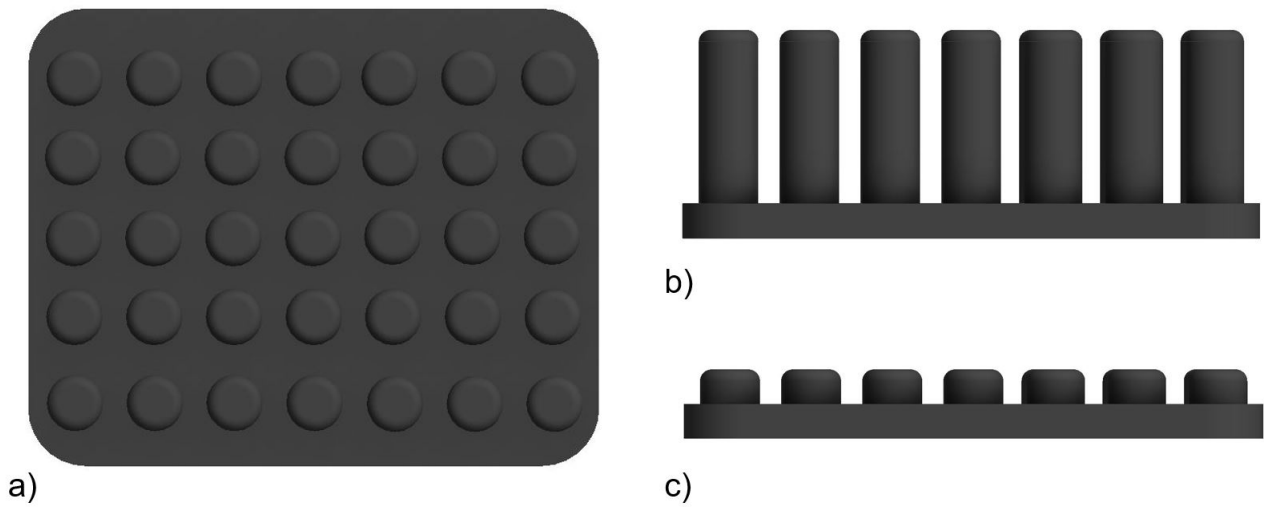


Fig. 20. CAD models of electrodes with pins: a) top view, b) side view of the electrode with long pins, and c) side view of the electrode with short pins

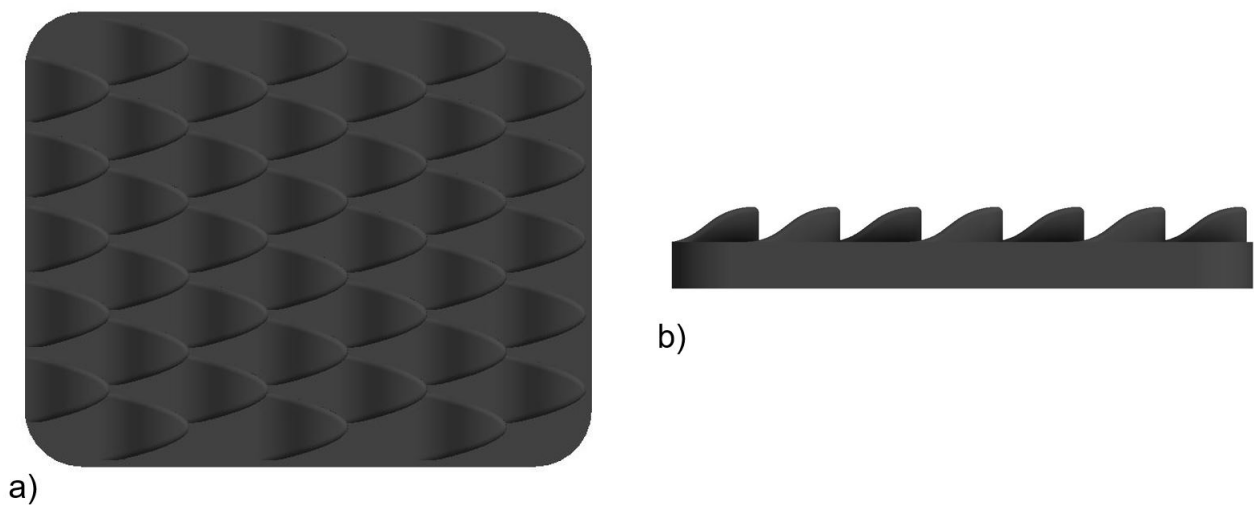


Fig. 21. CAD models of the electrode with a snake pattern: a) top view and b) side view of the electrode.

### C. Testing setup for impedance measurements

The testing setup for electrode impedance measurements consists of two Ag/AgCl plates, used for clamping the electrode (Fig. 22(a)). The impedance ( $Z$ ) of each electrode is measured by Zurich Instruments Impedance Analyzer, using the frequency sweep function.

For ESI measurements, pairs of electrodes are placed on the forearm (Fig. 22(b)), and the combined ESI is measured ( $Z_{measured}$ ). First, the ESI is measured for two wet Ag/AgCl electrodes in order to calculate the ESI of one wet electrode ( $Z_{wet}$ ). Then, the ESI of different pairs of one wet Ag/AgCl and one dry CNT/PDMS electrode is measured. The ESI of each dry electrode ( $Z_{dry}$ ) is calculated by subtracting the ESI of one wet electrode from the measured ESI:

$$Z_{measured} = Z_{wet} + Z_{dry}$$

The normalization of the ESI ( $Z_{normalized}$ ) by the projected area ( $A_{projected}$ ) is further calculated by:

$$Z_{normalized} = Z_{dry} \times A_{projected}$$

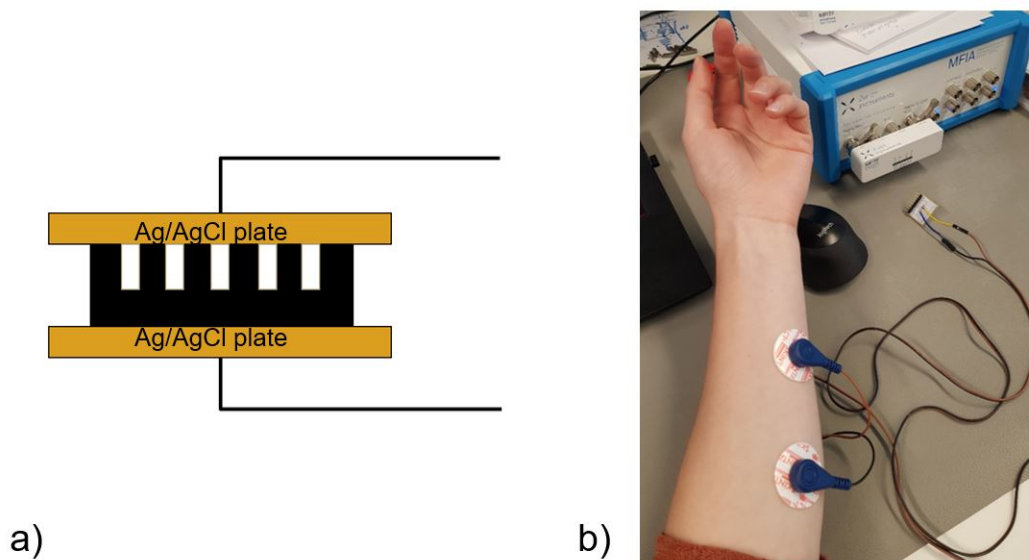


Fig. 22. Testing setups for a) electrode impedance measurements and b) ESI measurements.